Er addition to Al-Si-Mg-based casting alloy: Effects on microstructure, room and high temperature mechanical properties

Marco Colombo [a, *], Elisabetta Gariboldi [a], Alessandro Morri [b]

[a] *Politecnico di Milano, Department of Mechanical Engineering, Via La Masa 1, 20156 Milan, Italy*
[b] *Department of Industrial Engineering (DIN), Alma Mater Studiorum, University of Bologna, Viale Risorgimento 4, 40136 Bologna, Italy*

The paper deals with the production, heat treatment, microstructural and mechanical characterization of innovative Al-Si-Mg alloys based on Al-7Si-0.4 Mg (A356) with additions of rare earth Er, with the aim of increasing the microstructural stability and mechanical performances at high temperature. Three alloys with different Er concentration (between 0, and 0.41 wt%) were investigated in the as-cast, peak aged and overaged conditions. Microstructural analyses demonstrated that Er additions affect eutectic morphology by fragmenting and spheroidising Si particles. Tensile tests at RT, 423 and 473 K proved that Er-containing alloys have improved mechanical strength with respect to the reference alloy; in particular, among the investigated alloy, the one with 0.22 wt% Er displayed the best combination of mechanical properties in all the tested conditions. Additions of 0.41 wt% Er, on the other hand, led to reduced castability of the alloy, with increased fraction of casting defects, and to the formation of primary Er-rich precipitates with high aspect ratio, causing a drop in ductility and reduced mechanical properties. Tests results demonstrated the importance of suitable chemical additions in improving the mechanical behaviour of cast Al-Si-Mg alloys. It can be concluded that the alloy containing 0.22 wt % Er could be proposed for structural applications at room and elevated temperatures, effectively extending the operating temperatures of Al-Si-Mg-based alloys.

Keywords:
Al-7Si-0.4 Mg (A356) alloy
Erbium
Microstructure
Mechanical properties
Aging

1. Introduction

Al-Si-Mg alloys, due to their good specific strength, excellent castability and good corrosion resistance, are widely used in many industrial fields, particularly in the transportation sector. Relatively good mechanical properties can be obtained by solution heat treatment and artificial aging, which lead to the precipitation of nanometric strengthening particles in α-Al. In the underaged state, and up to the peak aged condition, strengthening of the alloys belonging to this system is due to a mixture of β'' (Mg_5Si_6) and of pre-β'' phases [1]. When further exposed at temperatures exceeding 423 K, a rapid evolution of strengthening phases takes place. They evolve losing coherency with the matrix and effectiveness in hindering dislocations [2], with a consequent fast reduction of mechanical properties. Retarding and slowing overaging phenomena by stabilization of the microstructure would improve the alloys mechanical properties, extending their application fields, also at high temperatures.

Literature studies reported that the mechanical properties, of Al-Si-Mg alloys are very effectively enhanced by the additions of rare earths [3–5]. Some of the added elements also showed a concomitant modification action on eutectic Si, similar to the one operated by Sr, leading to higher alloy ductility, as shown in Ref. [6] by *Shi* et al.

Among rare earth, Er proved to be an effective strengthening element for Al alloys [7–9]. The effect of Er can be explained by the precipitation of nanometric $L1_2$ Al_3Er dispersoids that, due to their crystallographic coherency with Al and their low coarsening rates, are very effective in retarding dislocations motions. Recent studies have focused on the addition of Er to Al-Si-Mg-(Cu) hypoeutectic or eutectic alloys [6,10], showing improved yield stress (YS), ultimate tensile strength (UTS) and elongation to fracture (ε%) of Er-containing alloys after room temperature tensile tests. Nevertheless, to the authors' knowledge, there is a lack of information about their high temperature mechanical properties as well as about their microstructural stability when exposed for a long time at high

* Corresponding author.
E-*mail addresses:* marco1.colombo@polimi.it (M. Colombo), elisabetta.gariboldi@polimi.it (E. Gariboldi), alessandro.morri4@unibo.it (A. Morri).

Published Journal Article available at: http://dx.doi.org/10.1016/j.jallcom.2017.03.076

temperatures.

Goals of this work were to investigate the effects of additions of limited amounts of Er on the microstructure and mechanical properties at different aging condition and temperatures of Al alloys based on a conventional Al-7Si-0.4 Mg (A356) casting alloy.

2. Materials and methods

Different amounts of Al-15 wt% Er master alloy were added to a commercial Al-7Si-0.4 Mg (A356) alloy, obtaining the chemical composition reported in Table 1. Two sets of alloys containing Er were studied: one with a low Er concentration (nominal 0.3 wt%, named E3) and the other containing high Er amount (nominal 0.6 wt%, named E6). It is important to underline that no modifying agent, like Sr or Na, was added to the alloys.

The reference and the master alloys were melted in an induction furnace at a temperature of 1073 K, under Ar atmosphere; the melt was magnetically stirred at this temperature for 30 min to improve its chemical homogeneity. It was then poured in a permanent steel mould, pre-heated at 473 K. The cast parts were in the form of cylinders, with a diameter of about 40 mm and 120 mm in height.

After casting, samples with the approximate dimensions of $10 \times 10 \times 10\ mm^3$ were extracted from similar positions of the cast bars for microstructural observations and hardness tests. A set of samples was analysed in the as-cast state, while another set was exposed at 813 K for 5 h with cold water quenching (SHT) and aged at 473 K for different times up to 168 h. Specimens were stored at 255 K for a maximum time of 30 min between SHT and aging to minimize microstructural evolution.

Samples for microstructural analyses were etched with Keller's reagent after conventional metallographic polishing. Optical micrographs were used to characterize the alloys microstructures and to identify general microstructural features (such as SDAS, eutectic morphology and porosity), evaluated by means of a free image analysis software (ImageJ). SDAS and eutectic morphology were used as indices of microstructural refinement and eutectic modification, respectively. SDAS was measured in the as-cast condition on 50× magnification micrographs, with a minimum of 100 measurements for each alloy (a total surface of about 6.8 mm^2 for each sample).

Eutectic morphology was characterized, in the as-cast and solution treated conditions, by measurements of Si major axis and aspect ratio, with each Si particle approximated as an ellipsoid. At least 1500 Si particles were analysed for each alloy and condition.

The alloys porosity was calculated by measuring the percent area fraction of defects on samples extracted from similar positions of the cast. Each value is obtained averaging the measurements performed on three 25× optical micrographs.

SEM micrographs and EDS analyses were carried out to acquire morphological and chemical data on the other intermetallic phases in the peak aged condition.

Vickers microhardness tests were performed with an applied load of 2.94 N; reported microhardness values are the average of at least 10 measurements.

Specimens for tensile tests with a circular cross section and collars were machined from the central part of the cast cylinders, in accordance with ASTM E8M-REV A specifications [11]. In particular, they were characterized by a gauge length of 30 mm and a gauge diameter 6 mm. Tensile tests were performed in the as-cast state at 298 K, in the peak aged condition at 298, 423 and 473 K and in the overaged condition (168 h at 473 K) at 298 and 473 K. Tensile tests were performed in displacement control mode, with a crosshead displacement rate of 0.017 mm/s. Due to the significant differences in ductility for the studied alloys, strain hardening exponents were calculated from a fixed region of the true plastic strain-true plastic stress curves, namely from yield stress to the lowest plastic strain leading to failure observed in experimental tests.

Analyses of fracture surfaces were carried out with SEM and optical microscopes, to correlate fracture mode/morphology to microstructural features of the alloys.

Table 1
Chemical composition (in wt %) of the alloys used in this work, measured via GDOES analyses (nominal Er concentration reported in brackets).

	Al	Si	Mg	Fe	Ti	B	Er
A356	92.26	7.02	0.41	0.07	0.14	0.01	–
E3	91.65	7.38	0.36	0.08	0.14	0.01	0.22 (0.3)
E6	92.18	7.21	0.32	0.08	0.11	0.01	0.41 (0.6)

3. Results

3.1. Microstructural characterization

The microstructures of the A356 and modified alloys in the as-cast condition are characterized by α Al dendrites, surrounded by eutectic Si (Fig. 1). Intermetallic phases, described in the following, are also present.

The results of SDAS measurements are listed in Table 2; it can be noticed that SDAS reduced as the concentration of Er in the alloy is increased.

From analyses of low magnification micrographs, it also emerged that casting defects are present in the form of interdendritic shrinkage porosity. Micrographs representative of casting defects in the three alloys are reported in Fig. 1d–f.

The results of porosity measurements (listed in Table 3) highlight that, while the effect of 0.22% wt additions of Er on E3 is negligible, the addition of 0.41% wt of Er induced a significant increase of the porosity in the E6 alloy with respect to the A356, with consequent effects on mechanical properties (see section 3.2) [12].

Er also influenced eutectic Si characteristics; there is, in fact, a strong morphological change in Si when Er is added. As it is shown in the higher magnification light optical micrographs in Fig. 2, the eutectic Si of E3 and E6 in the as-cast state is fragmented and spheroidised.

The results of measurements of length and aspect ratio of Si eutectic particles, summarized in Table 4, confirmed this effect.

A plate-like eutectic Si, with high average length and aspect ratio, characterized the reference alloy. The addition of Er reduced these morphological indexes of Si particles: with respect to the reference alloy, E3 has 80% shorter particles, with 85% lower aspect ratio; further addition of Er did not promote any further spheroidisation, as shown in the last column of Table 4.

Optical micrographs of the alloys after SHT are reported in Fig. 3. The high temperature exposure during solution heat treatment caused a partial spheroidisation and fragmentation of the eutectic Si in A356, as shown in Fig. 3a. The quantitative description of eutectic Si in SHT condition, summarized in Table 5, clearly shows in A356 a lower aspect ratio with respect to the as-cast condition. In the case of alloys E3 and E6, SHT induced no significant effect on the eutectic aspect ratio. On the other hand, the high temperature exposure led to an increase of Si eutectic size.

While in the A356 reference alloy only Fe-containing intermetallics β (Al_5FeSi) (Fig. 4a) with their typical acicular morphology [13] were observed, the Er-bearing alloys were further characterized by the presence of intermetallics containing Er. In E3 three families can be recognized: elongated needles located in the eutectic region (A in Fig. 4b), blocky-shaped intermetallics (B in Fig. 4b), and globular intermetallics (D in Fig. 4b) at the interface between eutectic Si (C in Fig. 4b) and α-Al. The microstructure of

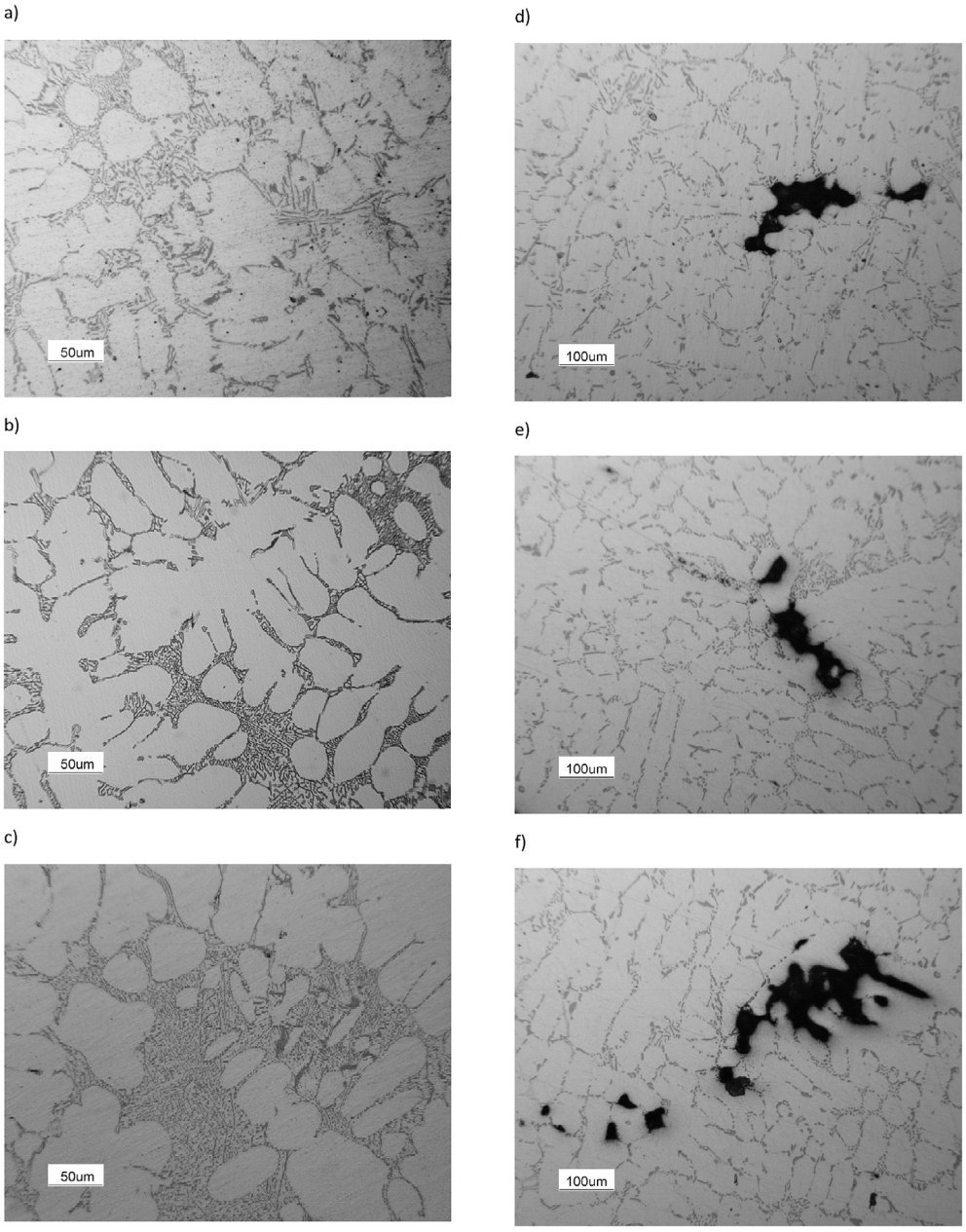

Fig. 1. Low magnification showing the microstructure of A356 (a), E3 (b) and E6 (c) alloys in the as-cast state and representative of the casting defects in A356 (d), E3 (e) and E6 (f).

Table 2
Measured SDAS for A356, E3 and E6 alloys.

	Measured SDAS (μm)
A356	31.5 ± 2.5
E3	24.1 ± 0.9
E6	22.8 ± 1.1

Table 3
Total area fraction of porosity of the three alloys.

	A356	E3	E6
Area fraction of defects	0.81% ± 0.2	1.07% ± 0.4	2.47% ± 0.7

alloy E6 (Fig. 4c) was characterized by a higher amount of the same kind of precipitates seen in alloy E3 (F in Fig. 4c), with the addition of complex shaped intermetallics (E in Fig. 4c). The average length of the latter was found to be of around 40 μm.

3.2. Mechanical properties

The aging response at 473 K of the investigated alloys is illustrated in Fig. 5, in terms of Vickers hardness vs. log aging time plot. In the quenched condition (i.e. no aging), the hardness of the three alloys was in the range 55–60 HV, increasing as a function of Er concentration. The peak aged condition was reached after about 3 h for all the alloys. The peak value of E3 and E6 alloys showed an increase of 14% and 19% with respect to the peak value of A356

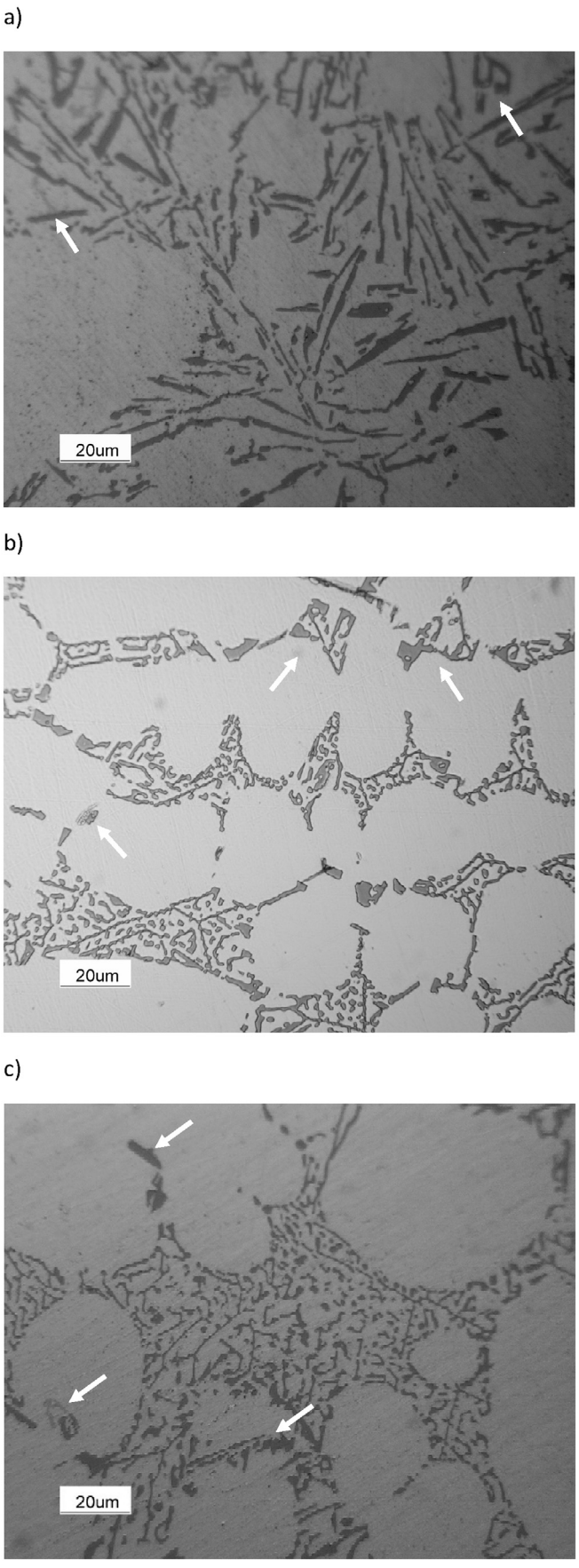

Fig. 2. High magnification light optical micrographs of A356 (a), E3 (b) and E6 (c), showing the effects of Er on Si eutectic dimensions and morphology. Arrows highlight intermetallics.

(about 97 HV). Overaging tests were interrupted after 168 h after which, for E3 and E6, relatively stable residual hardness values were reached. Residual hardness of E3 and E6 alloys were 28% and 36% higher than A356, respectively. In the overaged condition the hardness of the reference alloy decreased to a value close to that of the quenched condition. The tensile properties of the studied alloys are reported in Fig. 6 for the peak aged state and in Fig. 7 for the overaged condition. E3 displayed, for all the conditions, the highest strength and ductility.

Comparisons of the mechanical properties of the modified alloys with respect to A356 in the peak aged state showed that, at room temperature, YS increased of 20% and 2.5% for E3 and E6 alloys respectively. The UTS was increased of 14% for E3 while for E6 it was reduced of 9.6%. As regard ε%, E3 showed higher ductility, increased of 246.2%, while it was reduced of 15.4% for E6.

At 423 K, YS was increased of 22.7% and 11.3% for E3 and E6 respectively, UTS was increased of 21.8% and 6.6% for E3 and E6 respectively, but ε% was 155% higher for E3 and 45% lower for E6.

Finally, at 473 K, E3 showed a 27.1% higher YS, 24.7% higher UTS and 162% higher ε%, while E6 a 14.7% higher YS, 10.3% higher UTS and 19% higher ε%.

Strain hardening exponents are reported in Fig. 6d for the three alloys as a function of the testing temperature; it is shown that n is minimum in E3 alloy for all the testing temperatures and, generally, decreased as the testing temperature increased.

The improvement in mechanical properties of Er-containing alloys was even more evident in the overaged condition, particularly for E3 alloy. YS, UTS and ε% for E3 were increased at 298 K respectively of 28.2%, 39% and 51.4%, while at 473 K of 29.5%, 21%, and 71.6% respect to A356.

When considering E6, at room temperature the increase of YS and UTS were of 9.9% and 17.2% respectively, while ε% was reduced of 10.8%. At 473 K, E6 showed a 15.1% increase in YS, 4.6% increase in UTS and 12.2% increase in ε%.

Strain hardening exponents in the overaged condition are reported in Fig. 7c for the three alloys as a function of the testing temperature. A reduction in n as a function of the testing temperature was again observed, even though the numerical values in Fig. 7c are higher than those shown in Fig. 6d at a constant testing temperature. n exponent for E6 tested at room temperature in the overaged condition, differently from what was found in all the other temper conditions and testing temperatures, was lower than that of A356.

3.3. Fractographic analyses

Fracture analyses (Fig. 8) highlighted that in all alloys primary cracks nucleated and developed in the eutectic region, generating debonded and cracked Si particles. Similar path is followed by the secondary cracks that develop during the final stage of tensile tests (Fig. 8). In E6 samples, furthermore, primary and secondary cracks mainly propagate by linking large shrinkage porosities (Fig. 8c and f).

These observations and the higher amount of porosity in alloy E6 with respect to A356 and E3 can, therefore, explain the lower strength and ductility of this alloy. According to various authors [12,14–16], the amount of porosities on fracture surfaces of

Table 4
Geometric characteristics of eutectic Si for A356, E3 and E6 alloys in the as-cast state.

	A356	E3	E6
Si Aspect Ratio	10.8 ± 2.5	1.6 ± 0.5	2.4 ± 1.2
Si Average Length (μm)	27.2 ± 3.8	3.5 ± 0.6	4.1 ± 0.9

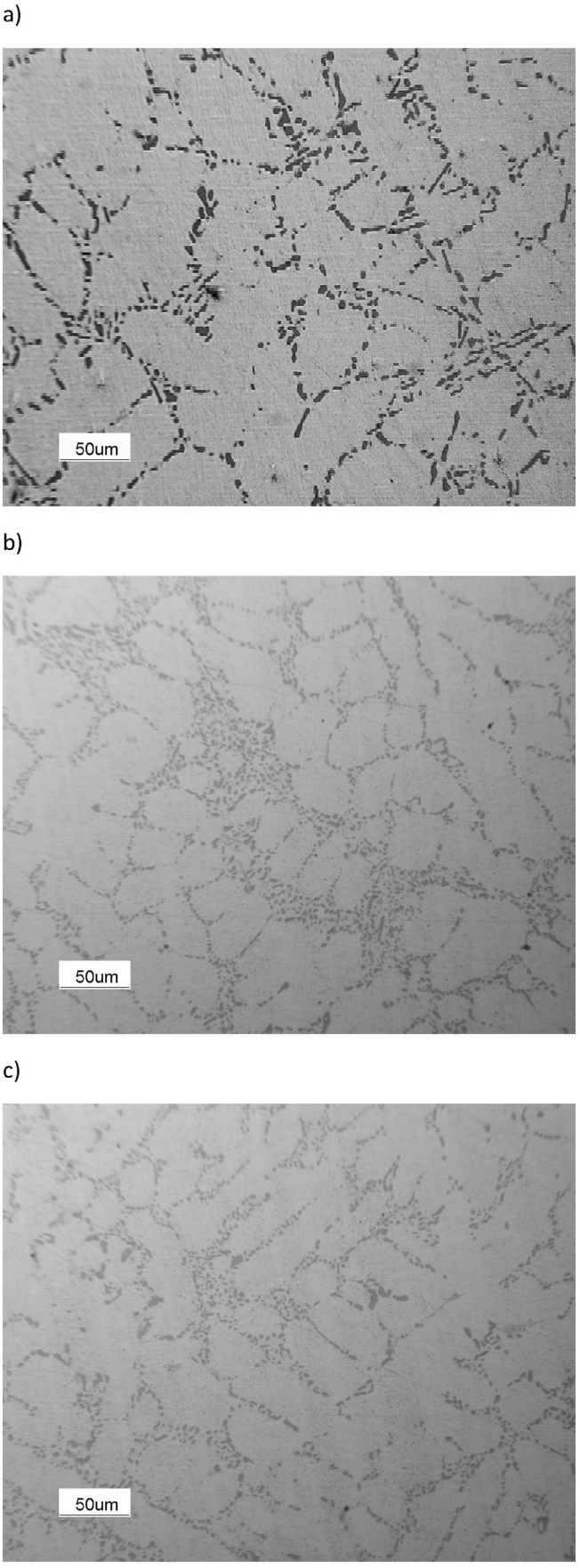

Fig. 3. Optical micrographs showing the effects of SHT on the eutectic of a) A356, b) E3 and c) E6.

aluminium casting alloys, in fact, is several times greater than mean fraction, and can effectively influence tensile strength and ductility of material.

These statements are confirmed by SEM fracture surface analysis of E6 tensile samples (Fig. 9), which highlighted the presence of an area fraction of pores larger than the mean value of 2.5% evaluated by means of optical micrographs.

4. Discussion

4.1. Microstructural characterization

The microstructural features of the investigated alloys will be hereafter discussed following the processing route, starting from solidification and cooling from casting to thermal treatment.

SDAS is usually correlated in literature to cooling rate during solidification (R, measured in °C/s), as described in Ref. [17] for A356 alloy and reported in equation (1):

$$SDAS = 39.4R^{-0.317} \quad (1)$$

where SDAS is measured in μm. The SDAS value for A356 reported in Table 3 enable to calculate a cooling rate of about 2 °C/s.

Since the casting parameters were not changed for the other alloys and their thermophysic properties can be considered only slightly affected by the low Er additions, this value can be regarded as representative also for E3 and E6 alloys. The SDAS refinement observed in Er-containing alloys should thus be related merely to compositional effects, in agreement with results reported by other authors [6,10]. The low solid solubility of Er in α-Al, shown in the Al-Er phase diagram reported in Ref. [18], and its low diffusion coefficient [19] caused its progressive enrichment at the interface between the just solidified α-Al dendrites and the liquid, with a concentration that may locally overcome the maximum solubility of Er in Al. This induce the precipitation of Er-containing intermetallics, as reported in Fig. 4b and c, that retard the dendritic growth, explaining the smaller microstructural dimensions for Er alloys [6]. In E6, the concentration of Er is higher than its solid solubility in Al at the eutectic temperature (reported to be 0.28 wt% at 913 K [20]), inducing the precipitation from the melt of primary Al_3Er precipitates at a temperature higher than the liquidus of the alloy; these could act as nucleating agents for α-Al dendrites. However, inoculation efficacy, as described in literature [6], is affected by two parameters: the similarity in crystal symmetry and a low lattice mismatch between inoculant and parent phase. Al_3Er precipitates have a $L1_2$ group symmetry, as α-Al, but a relevant lattice parameter mismatch (around 4%, as reported in Ref. [20]), which makes Al_3Er not so powerful as inoculation agent. This could explain the low reduction in SDAS for E6 with respect to E3.

The analyses of low magnification micrographs, also revealed that alloy E6 was characterized by a higher amount of interdendritic shrinkage porosity (Table 3 and Fig. 1d–f). The overcoming of the maximum Er solubility in α-Al seems to reduce the fluidity of the alloy; this could be probably due to the precipitation of primary Er-containing intermetallics that prevent the complete feeding of interdendritic regions resulting in higher interdendritic porosity, similarly to what was found in literature for Al_5FeSi intermetallics

Table 5
Parameters for the morphological description of eutectic Si for A356, E3 and E6 alloys after SHT.

	A356	E3	E6
Aspect Ratio	4.2 ± 1.2	1.2 ± 0.2	1.6 ± 0.5
Average Length (μm)	9.2 ± 1.8	4.5 ± 0.7	5.2 ± 0.9

a)

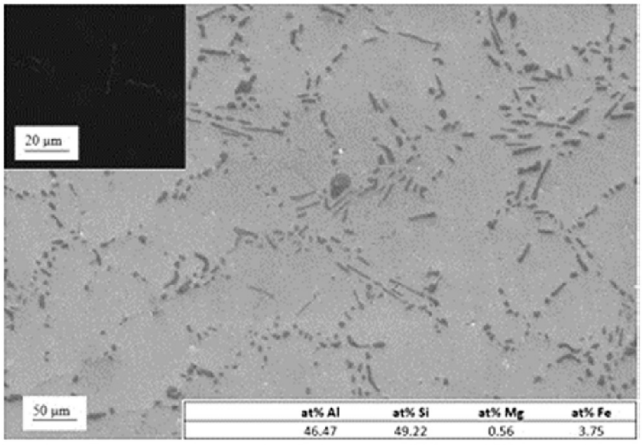

at% Al	at% Si	at% Mg	at% Fe
46.47	49.22	0.56	3.75

b)

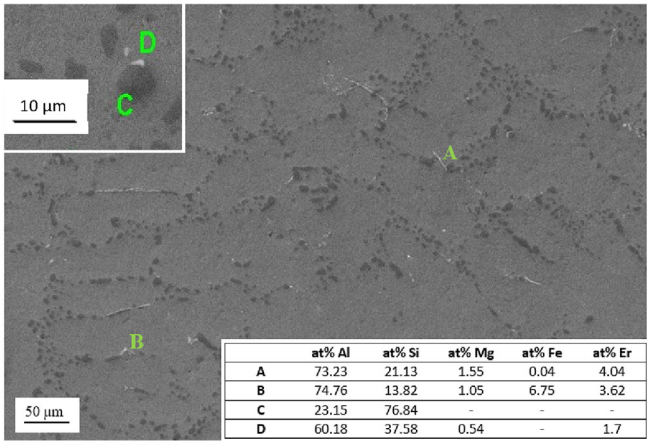

	at% Al	at% Si	at% Mg	at% Fe	at% Er
A	73.23	21.13	1.55	0.04	4.04
B	74.76	13.82	1.05	6.75	3.62
C	23.15	76.84	-	-	-
D	60.18	37.58	0.54	-	1.7

c)

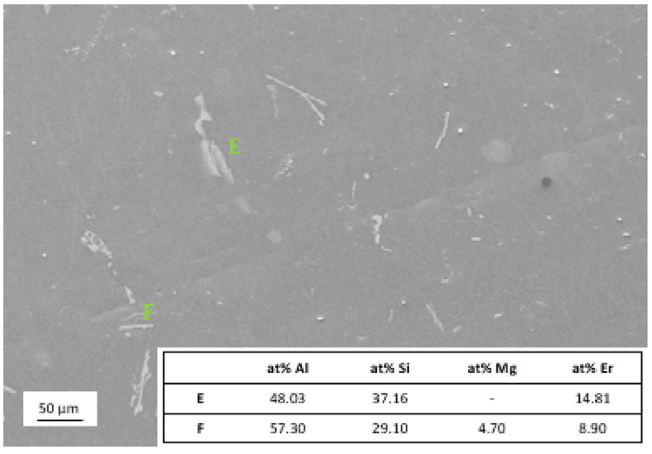

	at% Al	at% Si	at% Mg	at% Er
E	48.03	37.16	-	14.81
F	57.30	29.10	4.70	8.90

Fig. 4. Mixed BSE/SE micrographs showing the microstructure of a) A356, b) E3 and c) E6 alloys in the peak aged condition. The BSE/SE signal ratio is increased in c) to better highlight the different intermetallics. Higher magnification micrographs showing small intermetallics are reported as insets in the micrograph of the correspondent alloy. Also, EDS analyses of the representative intermetallics are reported in the same figure.

[21].

As far as eutectic modification is concerned, Er showed a marked effect in reducing the aspect ratio and length of Si, already in the as-cast condition. In A356 alloy, on the other hand, the eutectic is only locally and partially refined; since no modifier was added during casting, this is reasonably caused by the so-called "quench modi-fication" [22]. What emerged from Fig. 2 and Table 3 is that the modification effect did not increase linearly with Er concentration since, in E6, Si is not further spheroidised. This is possibly due to the overcoming of Er solubility in liquid Al, which causes the formation of primary precipitates that could reduce the amount of Er available for Si modification. There is no organic theory about the modifi-cation mechanism of Er for eutectic Si, which mechanism between poisoning of Twin-Plane Reentrant Edge (TPRE) or Impurity Induced Twinning (IIT) is acting and why there is an optimum Er concentration for Si modification. Specific studies on this topic, even if necessary for the development of Er-bearing Al-Si-alloys, are beyond the scopes of the present paper.

It could be reasonably assumed that further cooling to and storage at room temperature before thermal treatment or tensile tests did not significantly modify the microstructural features that could be investigated by optical/SEM analyses. Natural aging effects have been estimated in a previous work by some of the authors [23], leading to a hardness increase of about 5 HV during room temperature exposure of 1000 h for all the present alloys. This suggested that strengthening was mainly related to the beta precipitation sequences typical for A356 alloy, independently on the Er content.

It was demonstrated in Fig. 3 and Table 4 that SHT caused morphological changes of eutectic and intermetallics and a reduction in Si aspect ratio in all the alloys, more evident for A356. The high variability in Si aspect ratio, reported in Table 4 for A356, demonstrated that the spheroidisation caused by high temperature exposure is not homogeneous throughout the microstructure. Modified eutectic in Er-containing alloys, especially in E3, where Si aspect ratio and its variability were very low, contributed to higher alloy ductility, as demonstrated by tensile tests. As for eutectic Si dimensions, it can be observed that the eutectic length in A356 after SHT is lower than in the as-cast state, while for E3 and E6 it increased. This fact can be explained considering that two phenomena act on Si during SHT: fragmentation and coarsening. Fragmentation reduces the eutectic length and it is dominant in plate-like Si (as the one in A356), while coarsening is practically the only phenomenon acting in well modified coral-like Si (as the one in E3).

As far as intermetallics are concerned, the SHT caused fragmentation of β Fe-containing intermetallics (as shown in the inset of Fig. 4a). Comparing the EDS spectra of Er-rich intermetallics in E3 and E6 alloys, it is visible that the ones present in E6 are richer in Er than the ones present in E3. Identification of the phases in Er-containing alloys is not easy, partly due to their complex composition, to the lack of literature references such as complete phase diagrams for systems containing Er and studies on the effect of solidification rate. Considering the isotherm section of Al-Si-Er phase diagram at 873 K reported in Ref. [24], E3 and E6 should be in the Al + Si + τ_2 ($Er_2Al_3Si_2$) region. But the presence of Fe and Mg in the alloy and the lack of information on the evolution of chemical composition of intermetallic phases with temperature prevent from secure identification. Further, as it was shown in Fig. 4b and c, Er-rich intermetallics did not dissolve during SHT. This could be related both to their thermal stability and possibly to high particle/matrix interface energy, for which no data are available in literature.

The microstructural changes during aging, mainly connected to precipitation and evolution of nanometric strengthening particles,

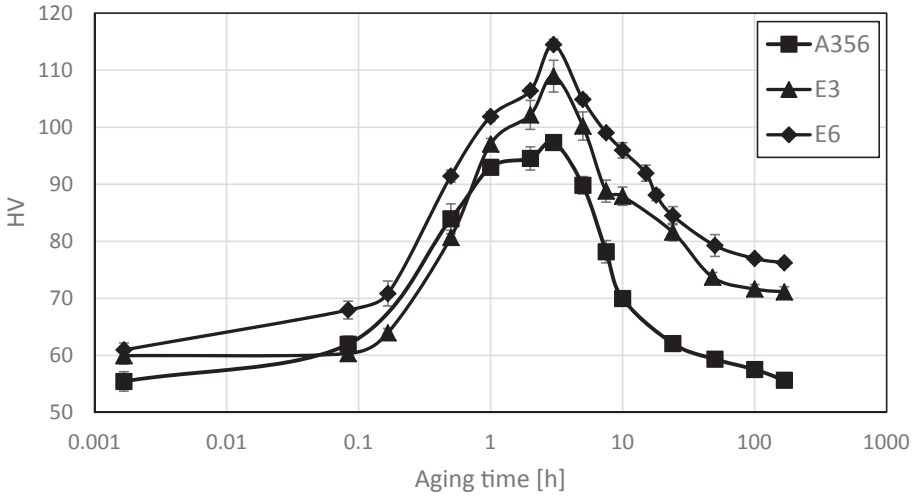

Fig. 5. Aging curves at 473 K for A356, E3 and E6. The initial point represents the microhardness value after quenching from SHT.

were indirectly correlated to the different mechanical properties obtained from hardness measurements and tensile tests.

4.2. Mechanical properties and fracture surfaces

The age-hardening response of the three investigated alloys, summarized in Fig. 5, clearly showed the beneficial effect of Er addition on peak hardness and on the alloy resistance to overaging.

The peak hardness increased as a function of Er concentration, in agreement with the results reported in Ref. [6]. This was related to the precipitation of Al_3Er dispersoids and the typical β" (Mg_5Si_6) of the reference alloy, as indicated in the XRD spectrum reported in Ref. [6].

The presence of Al_3Er precipitates, which are very resistant to coarsening, at least for temperatures up to 573 K [19], could also explain the larger difference of hardness between A356 and Er-containing alloys in the overaged state. The difference between E3 and E6 in the two aging conditions, on the other hand, is maintained almost constant, compatibly with the higher content of Er-rich coarse intermetallics of relatively stable amount and morphology in the E6 alloy [23], but further microstructural analyses are needed to confirm this latter point.

The presence of precipitate strengthening effect is also confirmed by the fact that the empirical equation relating YS of A356 in the as-cast state to SDAS [25]:

$$YS = -9.52ln(SDAS) + 115.8 \quad (2)$$

only holds for the reference alloys, as can be seen from Table 6 where YS for the three alloys were calculated using average SDAS values given in Table 2.

The YS higher than modelled for Er-containing alloys could be due to solid solution strengthening or to the precipitation of Er-containing particles during solidification. The higher amount of porosities in E6 with respect to E3 alloy could also have played a role in the difference between experimental and calculated YS.

When analysing the results of mechanical tests performed on heat treated specimen, it must be considered that the microstructural features discussed above (SDAS, morphology of eutectic Si, coarse intermetallics, strengthening intragranular particles and porosity) play different roles on mechanical properties.

Specifically, hardness and YS are mainly related to strengthening particles and secondary to other microstructural features; ductility, and in these brittle materials, UTS, are mainly affected by porosity, and in minor extent by the morphology of eutectic Si, coarse intermetallics and other microstructural features.

Coherently with literature, results of room temperature tensile tests, reported in Fig. 6a showed that the addition of Er in amount close to its maximum solubility in Al at the eutectic temperature can cause a relevant increase in the mechanical characteristics of Al-Si-Mg alloy, while overcoming this value is detrimental, causing a strong reduction in the alloy performances [6,10].

The analyses of tensile tests performed at high temperatures (Fig. 6b and c) indicated that Er is effective in increasing the thermal resistance of Al-Si-Mg alloys, which is probably caused by Er-rich, thermally stable precipitates, even though further microstructural analyses must be performed to have confirmations.

Tensile tests performed after 168 h of overaging (Fig. 7) supported the just mentioned hypothesis, indicating a strongly improved microstructural stability of Er-containing alloys, especially when considering E3.

Results about strain hardening exponents reported in Figs. 6d and 7c shows that n reduced with temperature. This is coherent with literature data and can be explained considering the facilitated movement of dislocations in the lattice as temperature increases and dynamic recovery [26].

It is also evident, comparing the value of n in different aging condition at a constant temperature, that prolonged aging caused an increase in the strain hardening ability of the materials, as mentioned in literature for overaging of age-hardenable alloys [27]. The increase in n is ascribable to the changes that occur in strengthening particles during overaging. The presence of incoherent strengthening particles, which resulted in a reduction in YS and UTS, caused the storage of dislocation loops around particles by means of Orowan looping, which influence the hardening ability of the alloy [27]. On the other hand, shareable precipitates can promote the localization of glide planes along deformation bands which, as the deformation proceeds, can intersect grain boundaries creating local stress concentrations which promote their opening [28].

The unexpectedly lower n value measured for alloy E6 tested at room temperature in the overaged condition could be explained considering the high amount of porosity shown in the micrographs reported in Figs. 8c, f and 9. High stress localization occurs at the pores tip, which induce strong localized plastic deformations and consequently the creation of dislocations. This caused a lowered

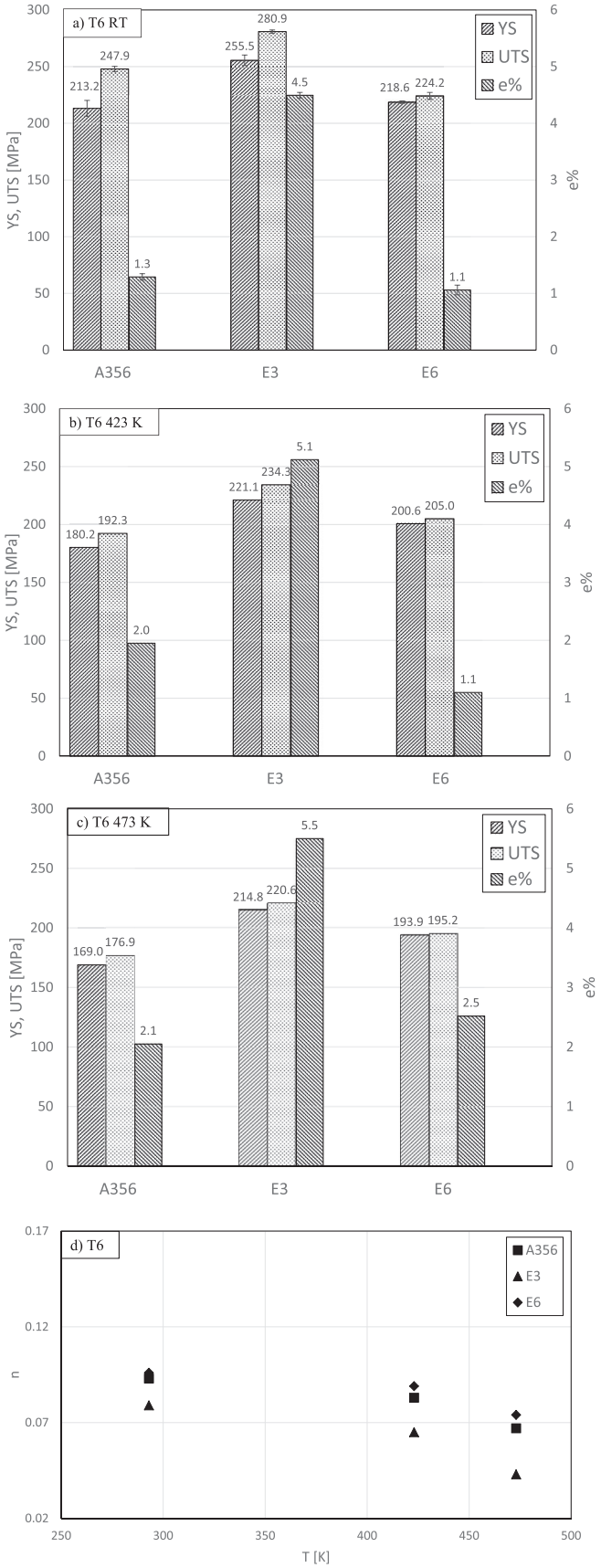

Fig. 6. Tensile properties of the investigated alloys in peak aged condition tested at a) room temperature (298 K), b) 423 K and c) 473 K. Strain hardening exponents for the alloys as a function of testing temperature are reported in d).

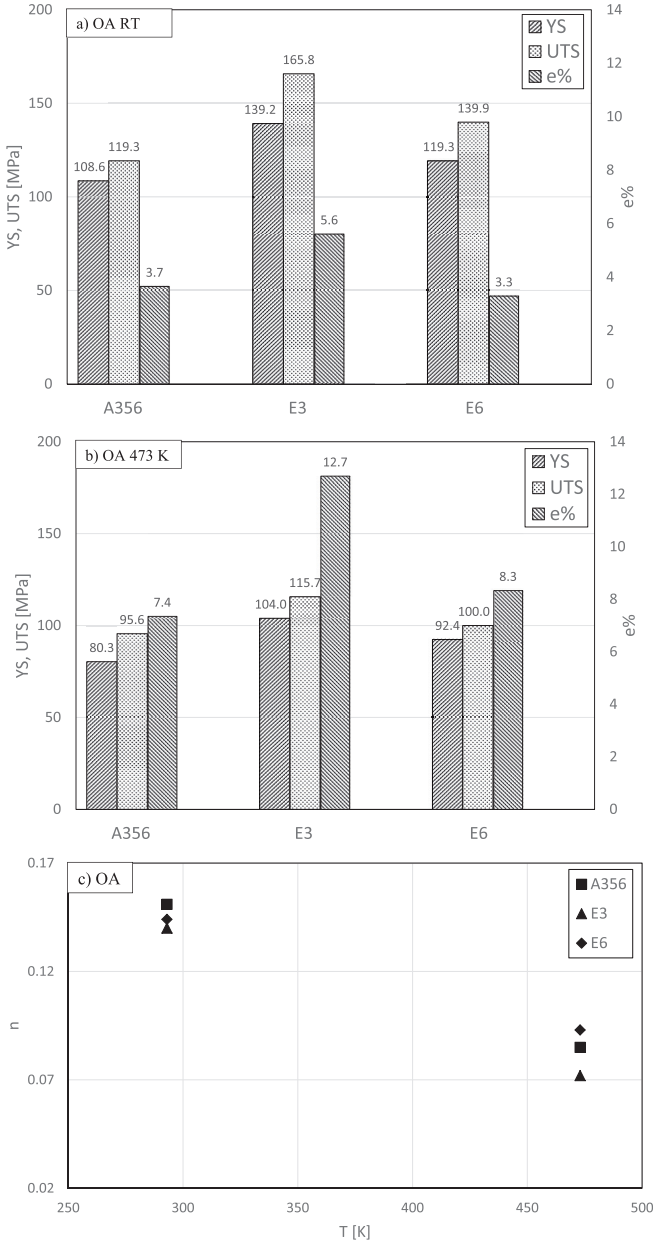

Fig. 7. Tensile properties of the investigated alloys overaged for 168 h at 473 K and tested at a) room temperature and b) 473 K. Strain hardening exponents for the alloys as a function of testing temperature are reported in c).

work hardening ability that resulted in a reduced n value.

To characterize the efficiency of thermal treatment in increasing the mechanical properties of the studied alloys, their room temperature YS in the heat-treated condition (reported in Figs. 6 and 7 and in the as-cast state (listed in Table 6) were subtracted. The subtraction is useful to remove the contribution of all the microstructural features that can influence YS, but that remain constant during thermal treatment, such as the one coming from SDAS.

Analyses on the results reported in Table 7 highlight that the highest gain in mechanical properties due to heat treatment is obtained for alloy E3, both for the peak aged and the overaged condition.

The YS differences with respect to as-cast condition reduces after overaging, as a consequence of the evolution of β" particles at the relatively high aging temperature adopted in the present

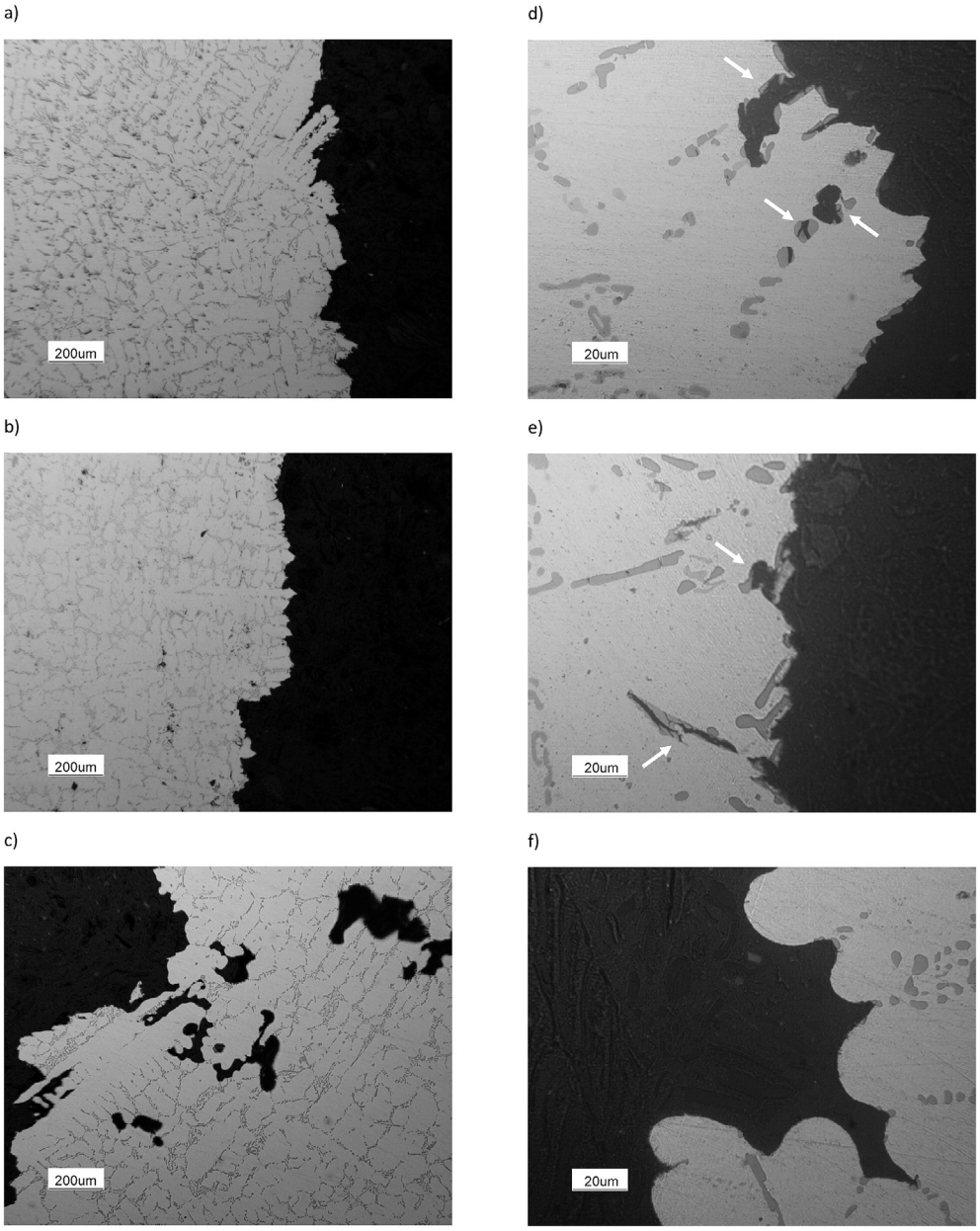

Fig. 8. Low magnification a), b) and c) and high magnification d), e) and f) fracture surfaces of A356, E3 and E6 respectively, tested at room temperature in the peak aged condition.

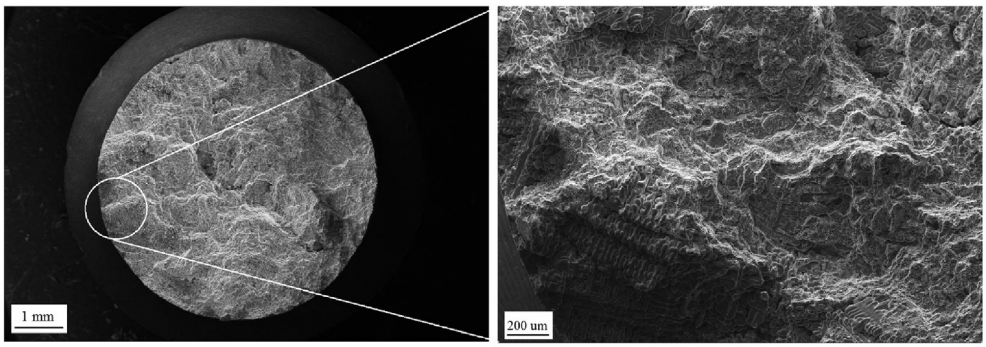

Fig. 9. Shrinkage porosity on the fracture surface of E6 alloy tested at room temperature in the overaged state.

Table 6
Comparison between experimental YS at room temperature for the investigated alloys in the as-cast state and those calculated from equation (2), using average SDAS values derived from microstructural analyses.

	Experimental YS [MPa]	Calculated YS [MPa]
A356	85.7	83.0
E3	92.5	85.5
E6	90.1	86.1

Table 7
Difference in room temperature YS between the heat treated (PA stands for peak aged, while OA for overaged) and the as-cast states.

	Condition	
	PA [MPa]	OA [MPa]
A356	127.5	32.4
E3	163	46.7
E6	128.5	26.2

investigation. The higher difference observed for E3 alloy is another indication of the beneficial effects of Er on the overaging resistance of Al-Si-Mg alloys, probably deriving from the coarsening resistance of Al_3Er precipitates [6,10], also confirming microhardness results. The low difference in the case of alloy E6 in OA condition could be induced by the presence of shrinkage defects close to the external surface of the specimen, as reported in the fracture surface in Figs. 8c, f and 9, which reduced the resistant area of the specimen, diminishing the alloy YS. The reduction in YS caused by porosity, despite lower than the reduction in UTS and ε%, has been reported in literature and could support this hypothesis [29,30].

Another information that can be extracted from tensile tests is the relative importance of porosity, eutectic spheroidisation and the presence of coarse intermetallics promoted by Er on material ductility and, consequently, on the UTS of these relatively brittle materials.

Cac`eres in Ref. [14] quantified the effect of porosity on the UTS and ε% on A356 alloy with simple mathematical models based on plasticity theory. Assuming that the proposed models are appli-cable also for A356-based E3 and E6 alloys, the influence of porosity on the mechanical resistance of the studied alloys can be estimated.

However, because amounts of porosity (Figs. 8 and 9) on cross sections both on and just below the fracture surfaces are higher respect to mean fraction evaluated from metallographic samples [14,31,32], the data in Table 8 could underestimate the effective reductions.

Due to the similar porosity levels for A356 and E3, it can be stated that the higher final resistance of E3 in all the testing conditions is related to strengthening precipitates, but also to the reduced aspect ratio of Si particles and the low amount of Er-containing intermetallics, which caused no significant local stress intensification action [31].

The increased porosity level (Table 8), and the presence of coarse intermetallics with high aspect ratio in E6 alloy caused a drop in ductility and UTS with respect to the E3 alloy in all testing conditions. The beneficial effect of eutectic modification prevailed over the stress localization caused by coarse intermetallics and porosity only at the highest temperature, both in PA and OA conditions. These statements are confirmed by fracture surface analyses which highlighted primary and secondary cracks propagating in eutectic regions, mainly by plastic bridges between solidification defects, and eutectic Si breaking, in accordance with fracture morphologies reported in literature [31].

Table 8
Effects of porosity on UTS and ε% for the studied alloys.

Alloy	Porosity	Reduction in UTS [14]	Reduction in ε% [14]
A356	0.81%	3%	30%
E3	1.07%	4%	40%
E6	2.47%	8%	60%

As a final remark, the present experimental study highlighted, among other findings, the need to combine the hardness response to tensile properties and microstructural characteristics when designing innovative age-hardening alloys. In fact, despite the highest hardness of the E6 alloy, its tensile properties and microstructural characteristics suggested that this is not suitable for structural applications. On the other hand, the low amount of primary precipitates in E3 alloy, together with other microstructural features, allowed this material to overcome 250 MPa YS and 4.1% in the T6 temper at room temperature, to show improved resistance to high temperature exposure and microstructural stability compared to the reference alloy.

5. Conclusions

The analyses of microstructural characteristics and mechanical properties of Al-Si-Mg alloys with Er additions led to the following findings:

- Er acted as a modifier for eutectic Si, effectively promoting its fragmentation and spheroidisation already in the as-cast state; Er also had an effect in reducing SDAS from a value of 31.5 μm for A356 to 22.8 μm for E6. Being the casting parameters constant, SDAS reduction must be related merely to compositional characteristics of the alloys,
- Er additions led to the formation of Er-containing primary intermetallics with elongated shape in inter-dendritic regions, which can cause a hardness increase but, above all, a reduction of alloys ductility, especially for E6,
- The addition of Er improved peak hardness and residual hardness after high temperature exposure with respect to A356. This is reasonably due to the formation of Er-containing strengthening and coarsening resistant precipitates, which also improved YS in all the testing conditions,
- The addition of 0.41 wt% Er (E6 alloy) greatly reduced the castability of the alloy, increasing the area fraction of pores to 2.47%, starting from 0.81% for the reference alloy. Porosity was found to influence ε%, UTS and also YS of the alloy, by reducing the effective resistant cross section of the specimens and inducing high stresses and plastic strains at the tip of pores,
- Among the investigated alloys, E3 showed the optimal combination of mechanical properties in the as-cast condition, as a consequence of microstructural refinement, eutectic Si modification, low amount of coarse embrittling Er-rich intermetallics and relatively reduced porosity. In addition to this well-balanced microstructure, the formation of thermally stable and coarsening resistant Er-containing dispersoids led to maximum improvement in mechanical properties also after thermal treatments.

References

[1] C.D. Marioara, S.J. Andersen, J. Jansen, H.W. Zandbergen, Atomic model for GP-zones in a 6082 Al–Mg–Si system, Acta Mater. 49 (2) (22 January 2001) 321–328, http://dx.doi.org/10.1016/S1359-6454(00)00302-5. ISSN 1359-6454.

[2] I. Polmear, J. David, Light Alloys: from Traditional Alloys to Nanocrystals, Butterworth-Heinemann, 2005.

[3] Y.-C. Tsai, C.-Y. Chou, S.-L. Lee, C.-K. Lin, J.-C. Lin, S.W. Lim, Effect of trace La

addition on the microstructures and mechanical properties of A356 (Al–7Si–0.35Mg) aluminum alloys, J. Alloys Compd. 487 (1–2) (13 November 2009) 157–162, http://dx.doi.org/10.1016/j.jallcom.2009.07.183. ISSN 0925-8388.
[4] S.L. Joy-Yii, D. Kurniawan, Effect of rare earth addition on microstructure and mechanical properties of Al-Si alloys: an overview, Adv. Mater. Res. 845 (2014) 27–30.
[5] R. Ahmad, M.B.A. Asmael, Influence of lanthanum on solidification, microstructure, and mechanical properties of eutectic Al-Si Piston alloy, J. Mater. Eng. Perform. 25 (7) (July 2016) 2799–2813, http://dx.doi.org/10.1007/s11665-016-2139-8.
[6] Z.M. Shi, Q. Wang, G. Zhao, R.Y. Zhang, Effects of erbium modification on the microstructure and mechanical properties of A356 aluminum alloys, Mater. Sci. Eng. A 626 (25 February 2015) 102–107, http://dx.doi.org/10.1016/j.msea.2014.12.062. ISSN 0921-5093.
[7] X. Chen, Z. Liu, S. Bai, Y. Li, L. Lin, Alloying behavior of erbium in an Al–Cu–Mg alloy, J. Alloys Compd. 505 (1) (27 August 2010) 201–205, http://dx.doi.org/10.1016/j.jallcom.2010.06.029. ISSN 0925-8388.
[8] S. Bai, Z. Liu, Y. Li, Y. Hou, X. Chen, Microstructures and fatigue fracture behavior of an Al–Cu–Mg–Ag alloy with addition of rare earth Er, Mater. Sci. Eng. A 527 (7–8) (25 March 2010) 1806–1814, http://dx.doi.org/10.1016/j.msea.2009.11.011. ISSN 0921-5093.
[9] Z.R. Nie, H. Huang, K.Y. Gao, B.L. Li, W. Wang, Z.Y. Chen, L. Rong, S.P. Wen, H.M. Li, T.Y. Zuo, The effect of erbium on the properties and microstructure of Al alloys, Mater. Sci. Forum 706–709 (2012) 329–334.
[10] X. Hu, F. Jiang, F. Ai, H. Yan, Effects of rare earth Er additions on microstructure development and mechanical properties of die-cast ADC12 aluminum alloy, J. Alloys Compd. 538 (15 October 2012) 21–27, http://dx.doi.org/10.1016/j.jallcom.2012.05.089. ISSN 0925-8388.
[11] Standard Test Methods for Tension Testing of Metallic Materials, ASTM standard, 2016.
[12] C. Do Lee, Effects of microporosity on tensile properties of A356 aluminum alloy, Mater. Sci. Eng. A 464 (1–2) (25 August 2007) 249–254, http://dx.doi.org/10.1016/j.msea.2007.01.130. ISSN 0921-5093.
[13] L. Ceschini, A. Morri, A. Morri, A study on the relationship between solidification conditions and microstructural characteristics of a complex shaped A356 gravity die cast cylinder head, in: Conf. Proc.. of the "5th Intern. Conf. High Tech Die Casting 2012-Innovation, Perspectives & Challenges in Pressure Die Casting of Light Alloys", AIM, Milano, 2012, pp. 1–12.
[14] C.H. Cáceres, On the effect of macroporosity on the tensile properties of the Al-7%Si-0.4%Mg casting alloy, Scr. Metall. Mater. 32 (11) (1995) 1851–1856, http://dx.doi.org/10.1016/0956-716X(95)00031-P. ISSN 0956-716X.
[15] A.M. Gokhale, G.R. Patel, Origins of variability in the fracture-related mechanical properties of a tilt-pour-permanent-mold cast Al-alloy, Scr. Mater. 52 (3) (February 2005) 237–241, http://dx.doi.org/10.1016/j.scriptamat.2004.09.011. ISSN 1359-6462.
[16] A. Morri, L. Ceschini, I. Svensson, S. Seifeddine, Relationship between Pores Volume (by Density Measurements) and Pores Area (on Fracture Surfaces) of A356 Fatigue Specimens, John Wiley & Sons, Inc., http://dx.doi.org/10.1002/9781118357002.ch31.
[17] L. Ceschini, A. Morri, A. Morri, A. Gamberini, S. Messieri, Correlation between ultimate tensile strength and solidification microstructure for the sand cast A357 aluminium alloy, Mater. Des. 30 (10) (December 2009) 4525–4531, http://dx.doi.org/10.1016/j.matdes.2009.05.012. ISSN 0261-3069.
[18] H. Okamoto, J. phase Equilib. Diffus. 32 (2011) 261, http://dx.doi.org/10.1007/s11669-011-9877-y.
[19] Y. Zhang, K. Gao, S. Wen, H. Huang, Z. Nie, D. Zhou, The study on the coarsening process and precipitation strengthening of Al3Er precipitate in Al–Er binary alloy, J. Alloys Compd. 610 (15 October 2014) 27–34, http://dx.doi.org/10.1016/j.jallcom.2014.04.093. ISSN 0925-8388.
[20] M.E. van Dalen, R.A. Karnesky, J.R. Cabotaje, D.C. Dunand, D.N. Seidman, Erbium and ytterbium solubilities and diffusivities in aluminum as determined by nanoscale characterization of precipitates, Acta Mater. 57 (14) (August 2009) 4081–4089, http://dx.doi.org/10.1016/j.actamat.2009.05.007. ISSN 1359-6454.
[21] M.A. Moustafa, Effect of iron content on the formation of β-Al5FeSi and porosity in Al–Si eutectic alloys, J. Mater. Process. Technol. 209 (1) (1 January 2009) 605–610, http://dx.doi.org/10.1016/j.jmatprotec.2008.02.073. ISSN 0924-0136.
[22] S. Hegde, K.N. Prabhu, Modification of eutectic silicon in Al–Si alloys, J. Mater. Sci. 43 (9) (2008) 3009–3027.
[23] E. Gariboldi, M. Colombo, Characterization of innovative Al-Si-Mg-based alloys for high temperature applications, Key Eng. Mater. 710 (2016) 53–58.
[24] V. Raghavan, Al-Er-Si (Aluminum-Erbium-Silicon), J. phase Equilib. Diffus. 31 (1) (2010) 44–45.
[25] M. Shabani, A. Mazahery, Prediction of mechanical properties of cast A356 alloy as a function of microstructure and cooling rate, Arch. Metall. Mater. 56 (3) (2011) 671.
[26] W.J. Poole, X. Wang, D.J. Lloyd, J.D. Embury, The shearable–non-shearable transition in Al–Mg–Si–Cu precipitation hardening alloys: implications on the distribution of slip, work hardening and fracture, Philos. Mag. 85 (2005) 3113–3135, http://dx.doi.org/10.1080/14786430500154935.
[27] P.A. Rometsch, G.B. Schaffer, An age hardening model for Al–7Si–Mg casting alloys, Mater. Sci. Eng. A 325 (1) (2002) 424–434, http://dx.doi.org/10.1016/S0921-5093(01)01479-4.
[28] J.D. Evense, N. Ryum, J.D. Embury, The intergranular fracture of AI–Mg–Si alloys, Mater. Sci. Eng. 18 (1975) 221–229.
[29] Z. Ma, A.M. Samuel, F.H. Samuel, H.W. Doty, S. Valtierra, A study of tensile properties in Al–Si–Cu and Al–Si–Mg alloys: effect of β-iron intermetallics and porosity, Mater. Sci. Eng. A 490 (1–2) (25 August 2008) 36–51, http://dx.doi.org/10.1016/j.msea.2008.01.028. ISSN 0921-5093.
[30] G.W. Mugica, D.O. Tovio, J.C. Cuyas, A.C. González, Effect of porosity on the tensile properties of low ductility aluminum alloys, Mater. Res. 7 (2) (2004) 221–229.
[31] Q.G. Wang, Microstructural effects on the tensile and fracture behavior of aluminum casting alloys A356/357, Metall. Mater. Trans. A 34A (2003) 2887–2899.
[32] K. Jha, K. Sreekumar, Effect of pores and acicular eutectic silicon particles on the performance of Al–Si–Mg (AS7G03) casting, Eng. Fail. Anal. 16 (2009) 2433–2439.